Electroencephalographic source reconstruction by the finite-element approximation of the elliptic Cauchy problem

Mikhail Malovichko, Nikolay Koshev, Nikolay Yavich, Alexandra Razorenova, and Maxim Fedorov

***Abstract*— *Objective*: This paper develops a novel approach for fast and reliable reconstruction of EEG sources in MRI-based head models. *Methods*: The inverse EEG problem is reduced to the Cauchy problem for an elliptic partial-derivative equation. The problem is transformed into a regularized minimax problem, which is directly approximated in a finite-element space. The resulting numerical method is efficient and easy to program. It eliminates the need to solve forward problems, which can be a tedious task. The method applies to complex anatomical head models, possibly containing holes in surfaces, anisotropic conductivity, and conductivity variations inside each tissue. The method has been verified on a spherical shell model and an MRI-based head. *Results*: Numerical experiments indicate high accuracy of localization of brain activations (both cortical potential and current) and rapid execution time. *Conclusion*: This study demonstrates that the proposed approach is feasible for EEG source analysis and can serve as a rapid and reliable tool for EEG source analysis. *Significance*: The significance of this study is that it develops a fast, accurate, and simple numerical method of EEG source analysis, applicable to almost arbitrary complex head models.**

***Index Terms*— Electroencephalography, source reconstruction, Cauchy problem, finite-element method.**

I. Introduction

ELECTROENCEPHALOGRAPHY (EEG) source localization with a head model based on individual MRI or CT scans has been an active area of research for preceding decades. A vast number of numerical methods have been proposed to date. The most universally recognized methods are those based on solving an inverse problem for underlying Poisson's equation.

The current-reconstruction algorithms seek to estimate the right-hand side of Poisson's equation (we refer to reviews [1]–[7], to mention a few). They are implemented in many free and commercial software packages, such as MNE suite, BrainStorm, FieldTrip, Curry, and some others. The algorithms in this group can be related to the Tikhonov minimization and include MNE family [8], [9], LORETA family [10], [11], LAURA [12], FOCUSS [13] among many other algorithms and their modifications. In the *cortically-constrained current reconstruction*, it is assumed that the source current is non-zero only on the cortex (also, the current is frequently considered normal to the cortex). It leads to a more stable solution [14], and many impressive examples of EEG source localization have been obtained by this approach [9], [15]. It can be demonstrated (see Section 2) that this problem is equivalent to the Cauchy problem for Poisson's equation.

The major drawback of all current-reconstruction methods is they require multiple solutions of the forward problem, which are typically arranged in the lead-field matrix. Accurate solution of the forward problem is a non-trivial task by itself, which also tends to become time-demanding on complex models.

Those implementations based on the boundary-element method (BEM) might not have enough geometric flexibility [16]. Typically, the head is represented with just a few compartments (e.g. scalp-skull-brain), which are closed (no holes). The conductivity is assumed isotropic and constant inside each compartment. The cortical surface is simplified significantly. Furthermore, the BEM results in a system of linear equations with a dense matrix, so the numerical complexity grows as $O(n^3)$ with problem size. Also, when the surfaces get close to each other, the system matrix becomes nearly singular. The numerical tests presented in [17] indicated that BEM might be slower than FEM in the case of fine-scale head models.

Implementations based on the finite-element method (FEM) can handle complex geometries and varying anisotropic conductivity. Various FE discretizations on tetrahedral/hexahedral grids have been applied to EEG simulation, such as classical H^1-conforming elements, mixed finite elements, discontinuous Galerkin, and others. Although many FE packages are available, an accurate numerical implementation of a FEM forward solver is still an elaborate task on its own, as indicated in the large number of articles [17]–[24] (among many others). A notoriously subtle point is the approximation of an $H^{-5/2}$ right-hand size (the dipole) in finite-element spaces. From a computational standpoint, it may become quite time-demanding on large grids (see [25]), since the number of the forward simulations needed to form the lead-field matrix is

The first and third authors were partially supported by the Russian Science Foundation, project No. 18-71-10071.

M. Malovichko and N. Yavich are with Center for Data-Intensive Science and Engineering (CDISE), Skolkovo Institute of Science and Technology, Moscow, Russia and also with Department of Computational Physics, Moscow Institute of Physics and Technology, Dolgoprudny, Russia, e-mail: m.malovichko@skoltech.ru

N. Koshev, A. Razorenova, and M. Fedorov are with CDISE, Skolkovo Institute of Science and Technology

equal to the number of electrodes minus one (we assume that the reciprocity principle is employed).

The potential propagation methods seek to propagate electric potential from the scalp inside the head through the sourceless domain. Such methods date back to at least the 1970s [26], [27]. Although these methods differ from each other in terms of implementation and application, it can be demonstrated that they solve the Cauchy problem for Laplace's equation. The majority of them are approximate in that they make various assumptions to link potential and its normal derivative on the scalp to that inside the head. For example, the skull resistivity is assumed negligible comparing to that of the scalp, or the head is approximated by a set of spheres (see [28]–[32]). These methods can be a part of more sophisticated algorithms [33].

Purely numerical potential-propagation algorithms exist. A BEM-based potential projection procedure was proposed in [34], [35]. In this approach, the forward problem is discretized by boundary elements and the cortical potential is computed as a pseudosolution of a system of linear equation with a dense rectangular matrix. More recently, an approach based on the mixed BEM formulation was proposed in [36]. It reconstructs both the normal current and the potential on the cortex. These approaches are appealing but still have some limitations rooted in the BE discretization, such as the inability to handle surfaces with holes and variations in conductivity inside compartments. Also, they require manipulation of large dense matrices, which can become time-demanding on fine grids.

Special mention should be made of *the deblurring* procedure by Gevins [37]. It maps the scalp potential to the cortex, making use of the FE discretization on tetrahedral grids (most likely, the standard H^1-conforming linear elements). This approach requires inverting a large submatrix of the stiffness matrix, which can be challenging. Technical details about this technology are scarce [38], [39].

In a broader mathematical context, there is extensive mathematical literature on the Cauchy problem for elliptic partial derivative equations. In relation to the inverse EEG problem, *the mixed quasi-reversibility method* of Bourgeois [40], [41] is of special interest. Originally developed for Laplace's equation, this method provides flexibility of the FEM and avoids the use of Green's operator(see Section 2). In [42], we apply this approach to the reconstruction of the cortical electric potential. Although this approach appeared prospective, it contains restrictive assumptions, such as the constant conductivity of the head, and the requirement to have measured data in many (tens of thousands) vertices of the grid.

This paper presents a method for reconstructing both potential and the current on the cortical surface given EEG measurements on the scalp. The approach is based on reducing the problem to an inverse boundary-value problem and application of the mixed quasi-reversibility method along with a finite-element (FE) discretization. In this paper, we removed a restrictive assumption of the constant conductivity in the head. It significantly improves the accuracy of the potential reconstruction and also allows to correctly approximate the electric current. We provided a constructive derivation of the mixed quasi-reversibility problem. We assess the accuracy of reconstruction on spherical and anatomical head models and provide some performance estimations. The interpolation from a small number of electrodes to a much bigger number of grid vertices is also addressed.

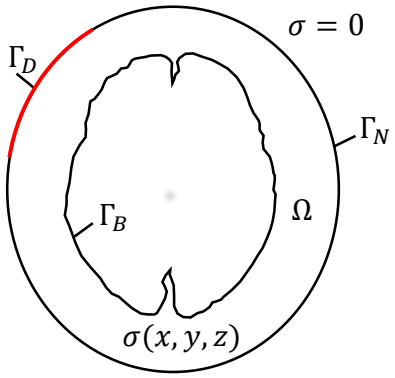

Fig. 1. Schematic representation of geometry. $\boldsymbol{\Gamma_D \subset \Gamma_N \subset \partial\Omega}$. Surface $\boldsymbol{\Gamma_B}$ may consist of a set of closed surfaces, e.g. the cortex can be represented by two disjoint surfaces.

The paper is organized as follows. In Section 2 we derive the continuous inverse problem. Section 3 is dedicated to its discretization and numerical implementation. Numerical experiments are presented in Section 4. Discussion and concluding remarks are given in Sections 5 and 6, respectively.

II. Problem Formulation

The electric potential inside the human head driven by the source current satisfies to Poisson's equation [16],

$$\begin{aligned} \operatorname{div}(\sigma \nabla u) &= \operatorname{div} J, \quad \text{in} \quad \Omega_0, \\ \left.\frac{\partial u}{\partial \nu}\right|_{\Gamma_N} &= 0. \end{aligned} \tag{1}$$

Here $\Omega_0 \subset \mathbb{R}^3$ is the head volume enclosed by surface Γ_N, u is the scalar electric potential, J is the source current (a vector field), σ is the electric conductivity, vector ν is a unit outward normal. Let the head be composed out of subdomains having sufficiently smooth boundaries. This assumption is general enough for quite complicated geometries, for example, a skull with openings and disjoint bones. We also assume that conductivity σ is a positive real-valued piecewise-analytic function uniformly bounded away from zero. The following interface conditions hold,

$$u_i = u_j, \quad \sigma_i \nabla u_i \cdot \nu = \sigma_j \nabla u_j \cdot \nu, \qquad \text{on } \Gamma_{ij}, \tag{2}$$

where indices i and j refer to any two neighboring subdomains with interface Γij. Problem (1) is well-posed (unique and stable) if the compatibility condition is satisfied. Let g_D be the potential measured on a part of the skin $\Gamma_D \subset \Gamma_N$. We want to reconstruct J assuming that it is non-zero only on the cortical surface, Γ_B. Here we presume that J is normal to Γ_B, though this condition will be removed later on.

We start our exposition with the classical current-reconstruction approach, which can be related to the Tikhonov minimization procedure,

$$\inf_{J,\varepsilon} \quad ||g_D - \mathcal{G}(J)||^2_{\mathcal{X}} + \varepsilon ||J||^2_{\mathcal{Y}}, \tag{3}$$

where $\mathcal{X}$ and $\mathcal{Y}$ are appropriate function spaces, $\varepsilon > 0$ is the regularization parameter, $\mathcal{G}$ is Green's operator, which computes $u|_{\Gamma_D}$ for given σ,J, and zero Neumann boundary conditions. If $\mathcal{X}$ and $\mathcal{Y}$ are Hilbert spaces, then (3) reduces to a linear problem for every ε. For example, if $\mathcal{X}$ and $\mathcal{Y}$ are L^2, then (3) after discretization reduces to the following linear problem for each ε,

$$(G^T G + \varepsilon I) j = G^T d, \tag{4}$$

where G is a discrete versions of operator $\mathcal{G}$ (the lead-field matrix), I is the identity matrix, j and d are discretized version of J and g_D, respectively. Many variants of this basic formulation have been described in the literature. In particular, $\mathcal{X}$ and $\mathcal{Y}$ can be merely Banach, the residual can be measured in a norm which accounts for the noise statistical properties, j can be subject to various priors. Similar formulations can be derived for reconstruction of the cortical potential [35], [37], and even both the potential and current [36]. In all the cases, the lead-field matrix G is the main ingredient. It is composed of the forward solutions for all candidate dipoles, so a forward solver, such as FEM, is necessary. The number of forward simulations required to compose the lead-field matrix for the cortically constrained case is equal to the number of electrodes minus one. In certain scenarios, the construction of the lead-field matrix implies a high computational cost. On the other hand, as soon as the lead-field matrix is constructed the rest of computations is fast.

Here we describe our approach. Let $\Omega \subset \Omega_0$ be a volume enclosed by the skin surface, Γ_N, and the cortical surface, Γ_B, such that $\partial\Omega = \Gamma_N \cup \Gamma_B$ (Figure 1). The normal current on a boundary can be interpreted as a dipole layer with some surface density, $S(\Gamma_B)$. That is, we have the following forward problem,

$$\begin{gathered} \operatorname{div}(\sigma \nabla u) = 0, \quad \text{in} \quad \Omega, \\ \left.\frac{\partial u}{\partial \nu}\right|_{\Gamma_N} = 0, \quad \sigma \left.\frac{\partial u}{\partial \nu}\right|_{\Gamma_B} = S. \end{gathered} \tag{5}$$

Problem (5) is understood in the weak sense, so conditions (2) are included in (5) by specifying the function spaces as $u \in H^1(\Omega)$, $\sigma\nabla u \in H_{div}(\Omega)$. We can specify formally $S \in H^{-1/2}(\Gamma_B)$, although much more smooth solutions appear in practice. The domain inside Γ_B does not impact the solution: the interior and exterior Neumann problems are uniquely determined by the double layer on the shared boundary (for example [43]). We can formulate an inverse problem, associated with (5), as follows.

$$\begin{gathered} \text{Find } S(\Gamma_B) \text{ provided} \\ \operatorname{div}(\sigma \nabla u) = 0 \text{ in} \quad \Omega, \\ \left.\frac{\partial u}{\partial \nu}\right|_{\Gamma_N} = 0, \ u|_{\Gamma_D} = g_D. \end{gathered} \tag{6}$$

Similarly, the interior and exterior Dirichlet problems are uniquely determined by the single layer potential on Γ_B. It motivates us to consider an inverse problem with respect to the potential, u, and then compute $S = \sigma\partial u/\partial\nu$. The problem reads,

$$\begin{gathered} \text{Find } u \text{ in } \Omega \text{ provided} \\ \operatorname{div}(\sigma \nabla u) = 0 \text{ in} \quad \Omega, \\ \left.\frac{\partial u}{\partial \nu}\right|_{\Gamma_N} = 0, \ u|_{\Gamma_D} = g_D. \end{gathered} \tag{7}$$

Given u, both $u|_{\Gamma_B}$ and S are computed by post-processing u. Note that, in (7), we do not assume that J is normal to Γ_B.

A note should be made on uniqueness of problem (7), which is the Cauchy problem for a linear elliptic PDE. Generally, the uniqueness of the Cauchy problem for elliptic PDEs with sufficiently smooth boundaries holds up to Lipschitz-continuous coefficients inclusively (see discussion in [44]). It is clearly not the case. However, the uniqueness of the Cauchy problem still holds for EEG, because the head consists out of several closed domains. The analytic continuation in each domain is unique due to Holmgren's theorem.

We apply the mixed quasi-reversibility method proposed in [40] to (7). The original method is formulated for the case $\sigma = 1$ and $\Gamma_D = \Gamma_N$, so we modified it. We propose a constructive derivation, applying the technique from [45].

Let $u \in H^1(\Omega)$, $g_D \in H^{1/2}(\Gamma_D)$ (the Dirichlet data). We apply the method of quasi-reversibility to problem (7), demanding boundedness of u in $H^1(\Omega)$ norm. Thus, we consider the following minimization problem,

$$\begin{gathered} \inf_{u \in H^1(\Omega)} \left(\frac{1}{2} \int_\Omega |\operatorname{div}(\sigma\nabla u)|^2 + \frac{\varepsilon}{2} \int_\Omega (|\nabla u|^2 + |u|^2) \right), \\ \text{s.t.} \ \ u|_{\Gamma_D} = g_D, \ \left.\frac{\partial u}{\partial \nu}\right|_{\Gamma_N} = 0, \end{gathered} \tag{8}$$

where $\varepsilon > 0$ is the regularization parameter. Here and below we omit the $\mathrm{d}x$ under the integral sign because the measure will be clear from the domain of integration. We observe that

$$\frac{1}{2} \int_\Omega |\operatorname{div}(\sigma\nabla u)|^2 = \sup_{q \in H^1(\Omega)} \left(-\int_\Omega q \operatorname{div}(\sigma\nabla u) - \frac{1}{2} \int_\Omega |q|^2 \right). \tag{9}$$

Next, the divergence theorem is applied to $\int_\Omega q \operatorname{div}(\sigma\nabla u)$. This is justified by the fact that $q \in H^1(\Omega)$, $\sigma\nabla u \in H_{div}(\Omega)$, and also it can be verified directly for smooth functions by applying the divergence theorem in each compartment and noting that surface integrals on the internal interfaces cancel out. We obtain the following minimax problem,

$$\begin{gathered} \inf_{u \in H^1(\Omega)} \sup_{q \in H^1(\Omega)} \left(\int_\Omega \sigma\nabla q \cdot \nabla u - \int_{\Gamma_B} \sigma q \frac{\partial u}{\partial \nu} - \frac{1}{2} \int_\Omega |q|^2 \right. \\ \left. + \frac{\varepsilon}{2} \int_\Omega (|\nabla u|^2 + |u|^2) \right), \text{s.t.} \ \ u|_{\Gamma_D} = g_D. \end{gathered} \tag{10}$$

Let us specify the following function spaces,

$$\begin{aligned} \tilde{V} &= \{v \in H^1(\Omega) : v|_{\Gamma_D} = g_D\}, \\ V &= \{v \in H^1(\Omega) : v|_{\Gamma_D} = 0\}. \end{aligned} \tag{11}$$

Then, problem (10) is equivalent to the following saddle-point

problem.

$$\begin{aligned} &\text{Find } (u,q)\in \tilde{V}\times H^1(\Omega) \text{ such that}\\ &\int_\Omega \sigma\nabla q\cdot\nabla v-\int_{\Gamma_B}\sigma q\frac{\partial v}{\partial \nu}+\varepsilon\int_\Omega(\nabla u\cdot\nabla v+uv)\\ &\qquad =0,\forall v\in V,\\ &\int_\Omega \sigma\nabla u\cdot\nabla\mu-\int_{\Gamma_B}\sigma\frac{\partial u}{\partial\nu}\mu-\int_\Omega q\mu=0,\\ &\qquad \forall\mu\in H^1(\Omega). \end{aligned} \tag{12}$$

Now we demand that q has zero trace on Γ_B, thus belonging to space

$$Q=\{v\in H^1(\Omega):v|_{\Gamma_B}=0\}. \tag{13}$$

Following [40] we stabilize (12) by demanding boundedness of $||q||_{H^1(\Omega)}$, that is, by adding term $-\delta\int_\Omega(q\mu+\nabla q\cdot\nabla\mu)$ to the second equation of (12). Since the norms $||q||_{L^2(\Omega)}$ and $\delta||q||_{L^2(\Omega)}$ are obviously equivalent for $\delta>0$, we omit term $-\int_\Omega q\mu$. Finally, we arrive to the following problem.

$$\begin{aligned} &\text{Find } (u,q)\in\tilde{V}\times Q \text{ such that}\\ &\int_\Omega\sigma\nabla q\cdot\nabla v+\varepsilon\int_\Omega(\nabla u\cdot\nabla v+uv)=0,\forall v\in V,\\ &\int_\Omega\sigma\nabla u\cdot\nabla\mu-\delta\int_\Omega(\nabla q\cdot\nabla\mu+q\mu)=0,\forall\mu\in Q, \end{aligned} \tag{14}$$

where $\varepsilon>0$ and $\delta>0$ are the two regularization parameters. Note that, the trace of u on boundary is specified, so $\int_\Omega|\nabla u|^2$ is a norm, which is equivalent to $||\cdot||_{H^1(\Omega)}$. Similarly, $\int_\Omega|\nabla q|^2$ is a norm in Q equivalent to $||q||_{H^1(\Omega)}$. So we might use in (14) the stabilizing terms $\int_\Omega\nabla u\cdot\nabla v$ and $\int_\Omega\nabla q\cdot\nabla\mu$, see [42].

In what follows, we solve (14) numerically by FEM.

III. Finite-element approximation and implementation

Domain Ω is divided into a set of tetrahedrons, $\mathcal{T}_h$, where h stands for the maximal diameter of tetrahedrons. We utilized the classical nodal-based linear basis functions $\mathcal{P}_1$. Let us introduce the following function spaces,

$$\begin{aligned} S_h&=\{v\in C^0(\Omega):v|_T\in\mathcal{P}_1\,\forall T\in\mathcal{T}_h\},\\ V_h&=\{v\in S_h:v|_{\Gamma_D}=0\},\\ \tilde{V}_h&=\{v\in S_h:v|_{\Gamma_D}=g_D\},\\ Q_h&=\{v\in S_h:v|_{\Gamma_B}=0\}. \end{aligned} \tag{15}$$

Problem (14) translates to the following discrete problem,

$$\begin{aligned} &\text{Find } (u_h,q_h)\in\tilde{V}_h\times Q_h \text{ such that } \forall(v_h,\mu_h)\in V_h\times Q_h\\ &\varepsilon\int_\Omega(u_hv_h+\nabla u_h\cdot\nabla v_h)+\int_\Omega\sigma\nabla q_h\cdot\nabla v_h=0,\\ &\int_\Omega\sigma\nabla u_h\cdot\nabla\mu_h-\delta\int_\Omega(q_h\mu_h+\nabla q_h\cdot\nabla\mu_h)=0. \end{aligned} \tag{16}$$

After assembling the system matrix and excluding essential degrees of freedom (DOFs), problem (16) is transformed into the following system of linear algebraic equations,

$$\begin{bmatrix} A & B^T\\ B & -C\end{bmatrix}\begin{bmatrix}x\\y\end{bmatrix}=f, \tag{17}$$

where block B corresponds the mixed bilinear form; blocks A and C correspond to the bilinear forms with ε and δ, respectively; vectors x and y correspond to free DOFs of u_h and q_h, respectively; non-zero entries of vector f are associated with the essential DOFs. Note that, q_h is an approximation of the divergence of Ohmic current, $\mathrm{div}(\sigma\nabla u)$, and should be close to zero. The system matrix in (17) is symmetric indefinite and invertible as long as A and C are positive-definite, that is, for $\varepsilon>0$, $\delta>0$. The matrix is sparse with its size is twice that of the number of vertices in the grid. We employ the sparse LU factorization to solve (17). To compute the current from u_h, we compute its approximation in $\tilde{V}_h$ following [46].

Our implementation is on C++ using MFEM library [47]. Computation of the element matrices is performed on the reference element making use of the Piola transformation. We employed UMFPACK sparse direct solver [48]. All computations reported in the present paper were serial.

IV. Numerical experiments

A. Spherical shell

The first numerical experiment was conducted with a spherical shell Ω enclosed by spheres S_a and S_b with the radii $a=1$ and $b=0.7$, respectively. The conductivity was set to $\sigma=1$ S/m. The potential in the volume Ω was computed as the solution to the following boundary-value problem,

$$\begin{aligned} &-\Delta u=0 \text{ in } \Omega,\\ u=g_D \text{ on } S_b,\quad &\frac{\partial u}{\partial\nu}=0, \text{ on } S_a, \end{aligned} \tag{18}$$

where g_D is a predefined potential on the inner sphere. Here the derivative operators understood in the classical sense. Problem (18) was solved by expanding the solution into spherical harmonics,

$$u(r,\phi,\theta)=\sum_{k=0}^{L}\sum_{m=-k}^{k}\left(A_{km}r^k+B_{km}r^{-k-1}\right)Y_k^m(\phi,\theta), \tag{19}$$

where Y_k^m are the spherical harmonics, and expansion coefficients A_{km} and B_{km} are determined from equations

$$\begin{aligned} A_{km}b^k+B_{km}b^{-k-1}&=\int_{S_b}g_DY_k^m,\\ kA_{km}a^{k-1}-(k+1)B_{km}a^{-k-2}&=0. \end{aligned} \tag{20}$$

We set $L=50$. To compute the right hand side of (20) we utilized quadratures and Matlab code by [49]. Accuracy of the computed quadrature was selected to ensure it integrates $\int_{S_b}Y_k^m$ with tolerance 10^{-7}. Domain Ω was discretized into 92,165 tetrahedrons (21,292 nodes) by Tetgen [50] via iso2mesh package [51]. Potential on the inner and outer surfaces are shown in Figure 2a,b.

Potential on the cortex, reconstructed with different values of ε and δ, is presented in Figure 2c. We observe that in all cases the algorithm reconstructed the pattern of the cortical activity, though with varying deviation.

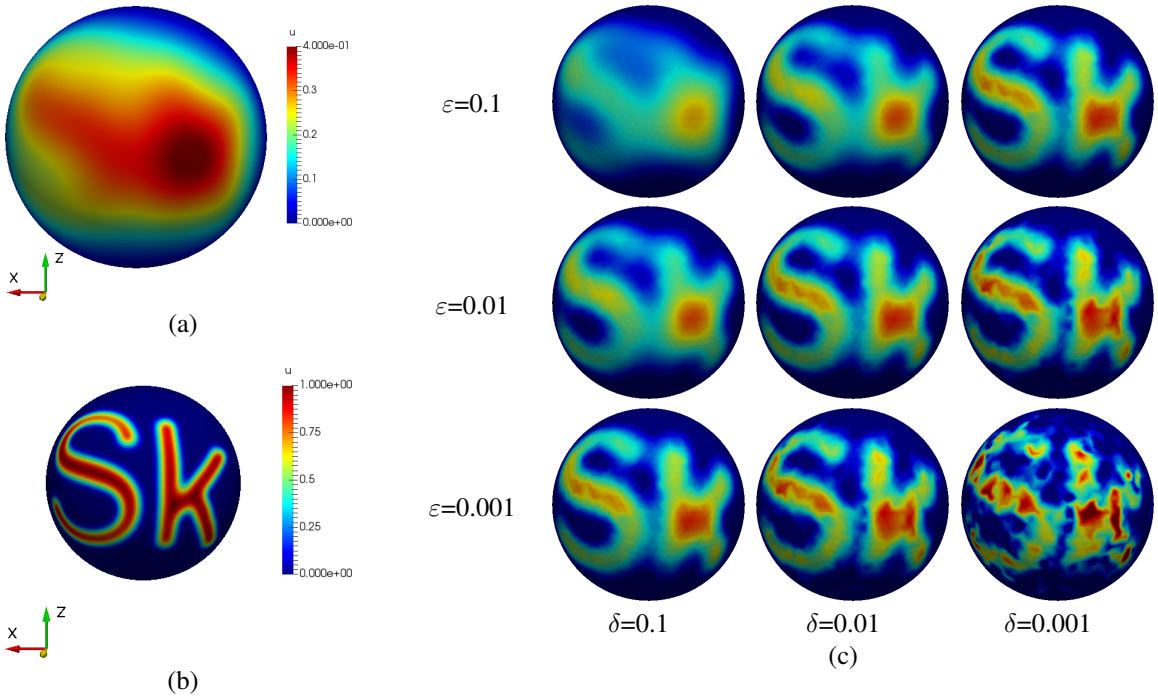

Fig. 2. The source reconstruction in a spherical shell. Panel (a). The true potential on the outer surface. Panel (b). The true potential on the inner surface. Panel (c). The potential on the inner sphere reconstructed from that on the outer sphere with different values of regularization parameters ε and δ. The color scales in (b) and (c) are identical.

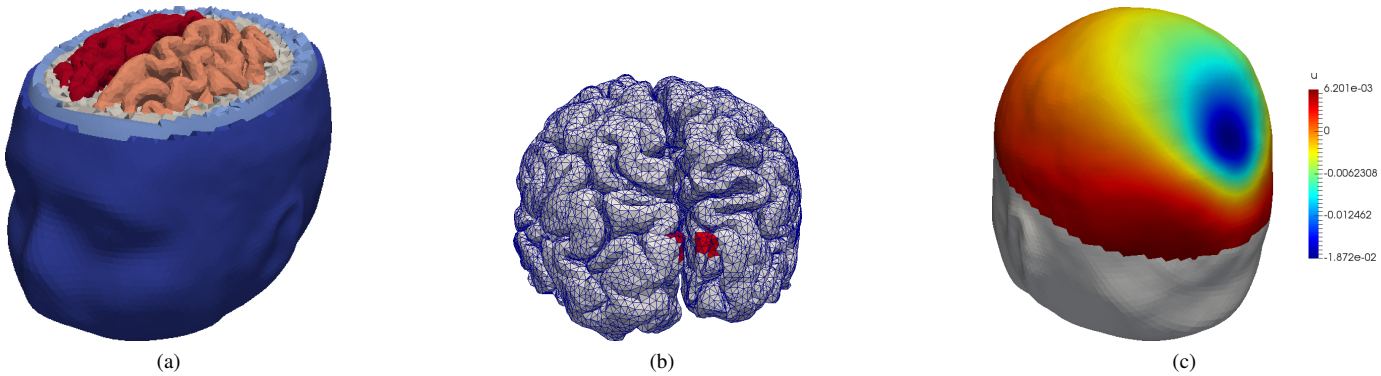

Fig. 3. Anatomical head used in the numerical experiment. Panel(a). The tetrahedral grid. Different tissues are shown in color. Panel(b). The true cortical sources. Tetrahedrons containing current dipoles are marked in red. Panel(c). Simulated electric potential on a part of the scalp (the Dirichlet data).

B. Anatomical head

In the second numerical experiment, we applied the algorithm to synthetic EEG data simulated over an anatomical head model. A participant's 3D head model was built from T1-weighted MRI volume obtained on a 1.5T Philips Intera system with 1 mm^3 resolution. Individual structural MRI scans were processed in FreeSurfer 4.3 suite [52] using the watershed segmentation algorithm. Surfaces of the skin, skull, and the cortical gray matter were loaded to iso2mesh package, processed and divided into a number of tetrahedrons. The tetrahedralization itself was performed internally by a call to TetGen mesh generator. The final grid, which consisted of the skin, skull, cerebrospinal fluid (CSF), and brain, contained 587,882 tetrahedrons (Figure 3).

The forward problem was solved by FEM using the conforming $\mathcal{P}_1$ elements. During the simulation, we assigned the following conductivities to the skin, skull, CSF, and brain to 0.33, 0.011, 1.0, and 0.33 S/m, respectively. The final grid consisted of 587,882 tetrahedrons (Figure 3a). The source dipoles were placed in 145 tetrahedrons adjacent to the two cortical patches in the visual cortex. The dipoles were located in barycenters of the tetrahedrons, oriented normally to the cortical surface and had unity moments (Figure 3b). The simulated distribution of potential on the scalp is shown in Figure 3c.

A grid for the inverse problem was produced by removing tetrahedrons assigned to the innermost compartment (the brain). Thus, the number of tetrahedrons was reduced to 354,669. The potential on a large part of the head surface

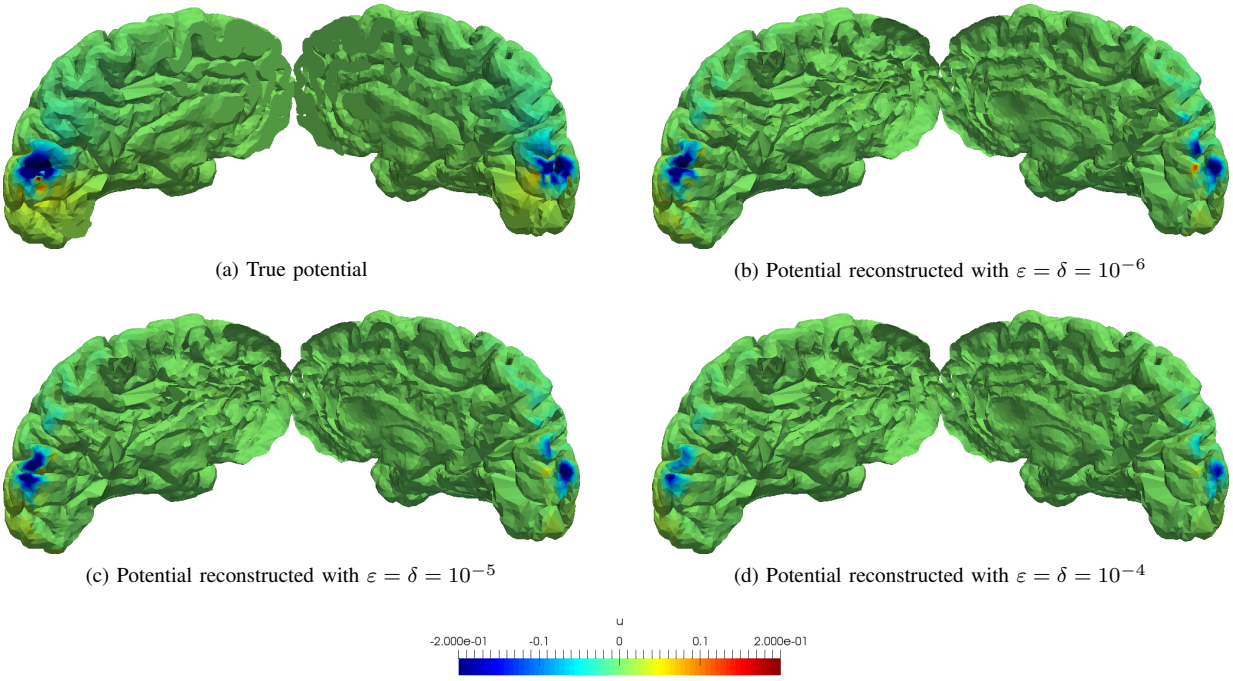

(a) True potential

(b) Potential reconstructed with $\varepsilon = \delta = 10^{-6}$

(c) Potential reconstructed with $\varepsilon = \delta = 10^{-5}$

(d) Potential reconstructed with $\varepsilon = \delta = 10^{-4}$

Fig. 4. Comparison of the true potential and the reconstructed one for different values of regularization parameters.

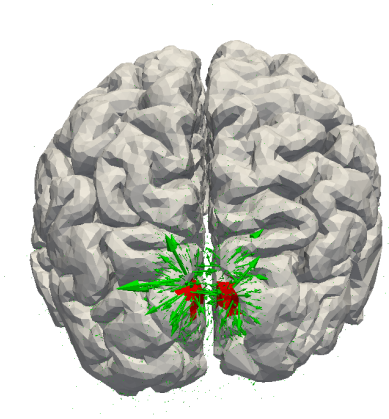

Fig. 5. Current reconstructed with $\boldsymbol{\varepsilon = \delta = 10^{-6}}$ (green arrows). Tetrahedrons containing the true current dipoles are marked in red.

were directly simulated by FEM (see Figure 3c) and then used as input (Dirichlet) data for the reconstruction algorithm. The potential reconstructed with different values of regularization parameters is shown in Figure 4. For all values of the regularization parameters, the most prominent feature is the high-amplitude area of negative potential in the visual cortex, which corresponds to the active patch. Its amplitude decrease as regularization parameters increase, but all localizations are consistent. In all cases, the reconstructed area is shifted towards the scalp, because the data could not properly resolve sources located in between the two hemispheres. The current for $\varepsilon = \delta = 10^{-6}$ is given in Figure 5. We observe a good localization of the active patches.

The fast solution of the system of linear equations is critical for the overall performance of the algorithm. Table I lists the performance of the direct sparse solver for different values of the regularization parameters. The code was run on a machine equipped with Intel Xeon CPU E5-2670 @ 2.6 GHz with 64 Gb RAM. The code was compiled by Intel C++ 19 compiler with flag -O3, and linked to MKL BLAS 2019 and SuiteSparse 5.6.0 libraries. All computations reported here were serial. The reported timing can be further improved.

TABLE I
PERFORMANCE OF THE DIRECT SPARSE SOLVER

ε,δ	Time,s	Memory, Gb
1E-6	1715	3.5
1E-5	1389	3.1
1E-4	626	2.5

Firstly, after the sparse LU (or Choletsky, or LDL^T) factors are computed, subsequent linear solves needed to process the whole EEG time series are inexpensive, so the timing in the table will be amortized. Secondly, the factorization itself can be accelerated using either shared-memory CPU parallelization or GPU units. Finally, application of preconditioned iterative solvers, which is a topic of an ongoing research, may dramatically accelerate computations.

In the following experiment, we evaluated the error due to restricting input data to a small number of electrodes. This feasibility test provides valuable insight, although the topic of interpolation noisy data on a complex surface requires a dedicated study. We extracted 175 electrodes located on the upper hemisphere of the 256-electrode Geodesic Sensor Net montage by Philips. The electrodes were projected on the scalp and adjusted to the nearest vertices of the grid using FieldTrip software [53]. The Dirichlet data were produced by interpolating the simulated potential from the electrodes to

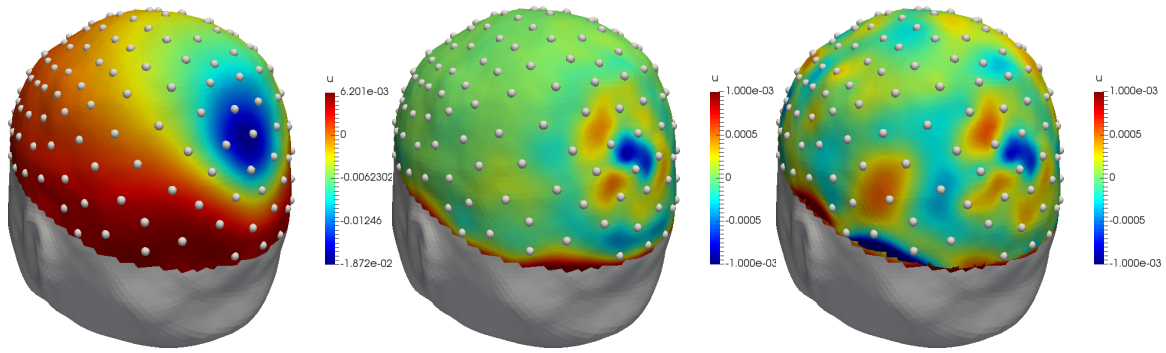

(a) (b) (c)

Fig. 6. Interpolation from the electrodes to mesh vertices. Panel (a). Dirichlet data interpolated from the noise-free electrode data. Panel (b). The error induced by the interpolation from the noise-free electrode data. Panel (c). The error induced by the interpolation from the noisy electrode data. The noisy Dirichlet data are not shown because the difference with panel (a) is hardly visible.

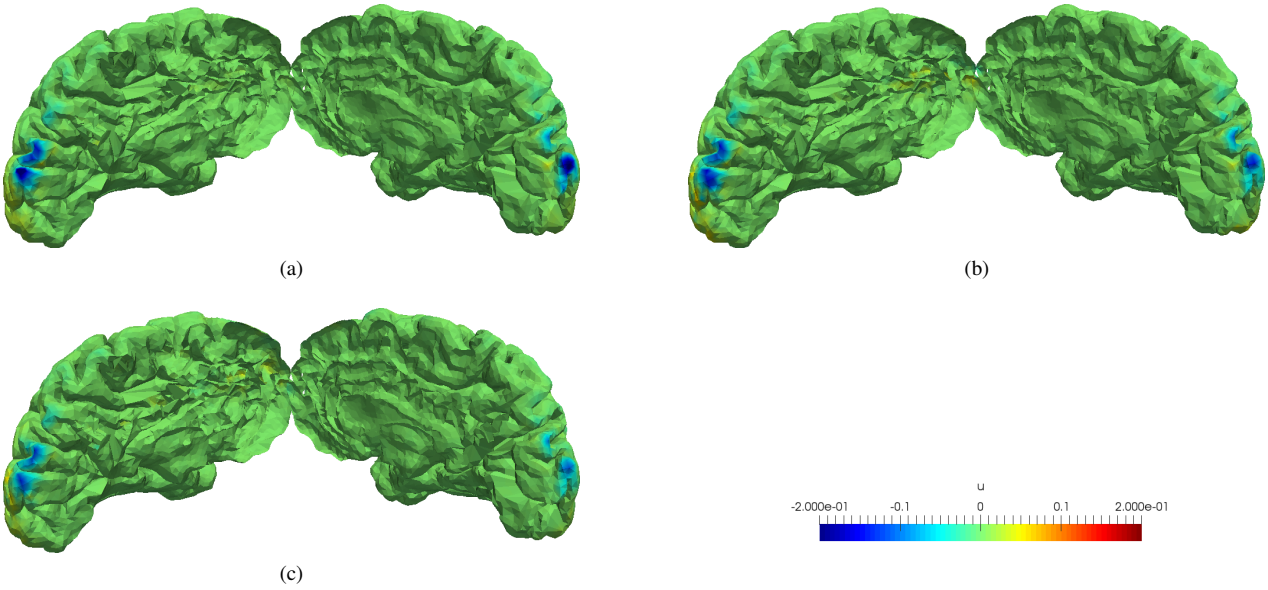

(a) (b) (c)

Fig. 7. Impact of the interpolation error, noise, and the choice of the grid on the source reconstruction. Panel (a): Dirichlet data were directly simulated by FEM in vertices of the grid. Panel (b): Dirichlet data were interpolated from noise-free electrode data. Panel (c): Dirichlet data were interpolated from the electrode data contaminated with 5% noise. In the first two case the forward and inversion grids coincided ("the inverse crime"), whereas in the last case the inverse grid differed from the forward one.

intermediate vertices of the grid with spherical splines [54], [55]. We used CSD Toolbox [56], [57], which was modified to interpolate data from the electrodes to arbitrary number of intermediate points and increase accuracy. The following parameter were used (see [55]): $m = 4$, $n = 10$, $\lambda = 0$. Head is not spherical, so this approach creates considerable non-stochastic error (Figure 6a,b). The reconstruction was performed with $\varepsilon = \delta = 10^{-4}$. The cortical potential, reconstructed from interpolated and the original data (Figure 7a,b), are consistent, although interpolated data resulted in a less pronounced active zone.

Finally, we added noise to the data and used a different grid in the reconstruction procedure to avoid the so-called inverse crime. The simulated potential on the electrodes was contaminated with Gaussian noise. The noise had zero mean and the standard deviation equal to 5% of that of the potential on the electrodes. The contaminated data were interpolated to the grid with exactly the same procedure as before. The grid used in the interpolation and, subsequently, reconstruction, differed from the simulation grid. It was resampled from the same surfaces but with different parameters totaling to 658,513 tetrahedrons. The reconstruction was performed with $\varepsilon = \delta = 10^{-4}$. Still, the potential on the cortex is consistent with the previous results (Figure 7c).

V. Discussion

The present paper proposes a novel numerical procedure for reconstructing the electric potential and current on the cortex from EEG data. The algorithm is based on the mixed quasi-reversibility method and a FE discretization. The regularized inverse problem is discretized in a finite-element space directly, resulting in a sparse system of linear equations. The advantage of the algorithm can be summarized as follows.

- Most notably, it does not rely on the solution of the forward problems. It dramatically simplifies a programming implementation and may reduce compute load, because the precomputation of the lead-field matrix is avoided.
- It works with complex geometries based on MRI scans, including ones with holes in the surfaces and disjoint tissues.
- The size of the problem is reduced by excluding the brain from the grid.
- The algorithm can be easily extended to anisotropic conductivity.
- Constraints in different function spaces are readily incorporated in the algorithm (we used $||\cdot||_{H^1}$ only).

Some caveats need to be outlined. First of all, the approach is limited to the case when the impressed current J is zero outside some boundary Γ_B (such as the cortex), including the case when Γ_B is a set of several disjoint surfaces (e.g. the two disjoint hemispheres). If J is attached to Γ_B, then the reconstructed Ohmic current on Γ_B is a discrete approximation of J, both normal and tangential components. If there are some sources inside Γ_B, their Ohmic current will contribute to the reconstructed value of J on Γ_B.

It is of interest to compare the presented method with FEM-based linear estimators (such as MNE) with a FEM-based forward solver. The forward solver can be of any type, such as the classical node-based elements, mixed FEM, discontinuous Galerkin, and others. Both approaches can handle almost arbitrary complex head geometries and material properties. The fundamental difference between them is that the latter explicitly build Green's operator to reduce the source reconstruction problem to a small discrete minimization problem. The presented method, in a sense, works in the other way round. It performs extension from discrete data to a trace of a function and then searches for a function in the head. The first approach provides flexibility because the candidate dipoles do not have to be restricted to a closed surface and can have arbitrary orientations. On the other hand, it becomes redundant if these restrictions are introduced. The candidate dipoles can be replaced with a dipole layer, the volume inside the surface is excluded from the grid and, eventually, Green's operator (a FEM forward solver) can be avoided altogether.

There are other choices of finite elements. Problem (7) can be reformulated with respect to the potential $u \in H^1(\Omega)$ and the Ohmic current $j = \sigma\nabla u \in H_{div}(\Omega)$. The pair (u, j) is then approximated in a $H^1(\Omega) \times H_{div}(\Omega)$-conforming finite-element space, as presented in [58]. The main advantage of this approach is the resulting discrete solution is conservative. On the other hand, the implementation is somewhat more involving. It should also be noted that if $\sigma = 1$, then problem (8) is essentially the biharmonic problem [45], for which a variety of discretizations is available.

Data interpolation is an important aspect. Real EEG data are measured with, at best, several hundred electrodes, so interpolation from electrodes to the surface of the head is necessary. This requirement is fundamental because specifying $g \in H^{1/2}(\Gamma_D)$ in a finite set of points on Γ_D does not define it uniquely. On the discrete level, a value of u_h on a boundary triangle is specified only if it is specified on the three vertices. Further work should include a study of the interpolation of data on a 3D surface.

Another open issue is the solution of the resulting system of linear equations, which comprises the bulk of the run time. Methods to accelerate this step need to be studied, in particular, parallel sparse direct solvers and preconditioned iterative solvers.

Finally, although the algorithm is theoretically stable, rigorous research on real noisy EEG data is necessary.

VI. Conclusion

This paper proposes a novel numerical procedure for reconstructing the electric potential and current on the cortex from EEG data. The algorithms is designed for a specific class of problems (cortically constrained source estimations), but very flexible in terms of the head geometry and material properties. The approach is based on the reduction of the regularized inverse problem to a saddle-point variational system, which is directly discretized in a finite-element space. The discrete solution is constructed with a single linear solve. Our results suggest that this approach can serve as a basis for fast and reliable cortically-constrained source reconstruction algorithms.

Acknowledgments

The authors acknowledge computational resources granted by University of Utah's Consortium for Electromagnetic Modeling and Inversion (CEMI); Complex for Simulation and Data Processing for Mega-Science Facilities at NRC "Kurchatov Institute", http://ckp.nrcki.ru/; and Skoltech CDISE's high-performance computing cluster, Zhores [59].

References

[1] S. Baillet, J. C. Mosher, and R. M. Leahy, "Electromagnetic brain mapping," *IEEE Signal Processing Magazine*, vol. 18, no. 6, pp. 14–30, 2001.

[2] C. Michel, M. Murray *et al.*, "EEG source imaging," *Clinical Neurophysiology*, vol. 115, pp. 2195 – 2222, 2004.

[3] L. Soufflet and P. H. Boeijinga, "Linear inverse solutions: Simulations from a realistic head model in MEG," *Brain Topography*, vol. 18, no. 2, pp. 87–99, Dec 2005.

[4] R.Grech, T. Cassar *et al.*, "Review on solving the inverse problem in EEG source analysis," *Journal of NeuroEngineering and Rehabilitation*, vol. 6, no. 25, 2008.

[5] R. D. Pascual-Marqui, K. Sekihara *et al.*, *Imaging the electric neuronal generators of EEG/MEG*. Cambridge University Press, 2009, p. 49–78.

[6] C. Michel and B. He, *EEG mapping and source imaging*. Lippincott Williams & Wilkins, 2010.

[7] S. P. Ahlfors and M. S. Hämäläinen, *MEG and EEG: source estimation*. Cambridge University Press, 2012, p. 257–286.

[8] M. S. Hämäläinen and R. J. Ilmoniemi, "Interpreting magnetic fields of the brain: minimum norm estimates," *Medical & Biological Engineering & Computing*, vol. 32, no. 1, pp. 35–42, Jan 1994.

[9] F. Lin, T. Witzel *et al.*, "Assessing and improving the spatial accuracy in MEG source localization by depth-weighted minimum-norm estimates," *NeuroImage*, vol. 31, no. 1, pp. 160 – 171, 2006.

[10] R. Pascual-Marqui, C. Michel, and D. Lehman, "Low resolution electromagnetic tomography: a new method for localizing electrical activity in the brain," *Int.J. Psychophysiol.*, vol. 18, pp. 49 – 65, 1994.

[11] R. Pascual-Marqui, "Standardized low-resolution brain electromagnetic tomography (sLORETA): technical details," *Methods Find. Exp. Clin. Phar- macol. (Suppl. D)*, vol. 24, pp. 5 – 12, 2002.

[12] R. De Peralta-Menendez, M. Murray *et al.*, "Electrical neuroimaging based on biophysical constraints," *Neuroimage*, vol. 21, no. 2, pp. 527–539, 2004.

[13] I. F. Gorodnitsky, J. S. George, and B. D. Rao, "Neuromagnetic source imaging with FOCUSS: a recursive weighted minimum norm algorithm," *Electroencephalography and Clinical Neurophysiology*, vol. 95, no. 4, pp. 231 – 251, 1995.

[14] A. M. Dale and M. I. Sereno, "Improved localization of cortical activity by combining EEG and MEG with MRI cortical surface reconstruction: A linear approach," *Journal of Cognitive Neuroscience*, vol. 5, no. 2, pp. 162–176, 1993.

[15] M. Fuchs, M. Wagner *et al.*, "Linear and nonlinear current density reconstructions," *J. Clin. Neurophysiol.*, vol. 16, pp. 267–295, 1999.

[16] J. De Munck, C. Wolters, and M. Clerc, *EEG and MEG: forward modeling*. CUP/BRRR, 2012, ch. Chapter 6, pp. 203–272.

[17] S. Pursiainen, A. Sorrentino *et al.*, "Forward simulation and inverse dipole localization with the lowest order Raviart—Thomas elements for electroencephalography," *Inverse Problems*, vol. 27, no. 4, p. 045003, mar 2011.

[18] Y. Yan, P. L. Nunez, and R. T. Hart, "Finite-element model of the human head: scalp potentials due to dipole sources," *Medical and Biological Engineering and Computing*, vol. 29, no. 5, Sep 1991.

[19] H. Buchner, G. Knoll *et al.*, "Inverse localization of electric dipole current sources in finite element models of the human head," *Electroencephalography and clinical neurophysiology*, no. 102, pp. 267–278, 1997.

[20] C. H. Wolters, H. Köstler *et al.*, "Numerical mathematics of the subtraction method for the modeling of a current dipole in EEG source reconstruction using finite element head models," *SIAM Journal on Scientific Computing*, vol. 30, no. 1, pp. 24–45, 2008.

[21] C. Engwer, J. Vorwerk *et al.*, "A Discontinuous Galerkin method to solve the EEG forward problem using the subtraction approach," *SIAM Journal on Scientific Computing*, vol. 39, no. 1, pp. B138–B164, 2017.

[22] J. Vorwerk, C. Engwer *et al.*, "A mixed finite element method to solve the EEG forward problem," *IEEE Transactions on Medical Imaging*, vol. 36, no. 4, pp. 930–941, 2017.

[23] M. C. Piastra, A. Nüßing *et al.*, "The discontinuous Galerkin finite element method for solving the MEG and the combined MEG/EEG forward problem," *Frontiers in Neuroscience*, vol. 12, p. 30, 2018.

[24] T. Miinalainen, A. Rezaei *et al.*, "A realistic, accurate and fast source modeling approach for the EEG forward problem," *NeuroImage*, vol. 184, pp. 56 – 67, 2019.

[25] Y. Huang, L. C. Parra, and S. Haufe, "The New York head — a precise standardized volume conductor model for EEG source localization and tES targeting," *NeuroImage*, vol. 140, pp. 150 – 162, 2016, transcranial electric stimulation (tES) and Neuroimaging.

[26] C. Nicholson, "Theoretical analysis of field potentials in anisotropic ensembles of neuronal elements," *IEEE Transactions on Biomedical Engineering*, vol. BME-20, no. 4, pp. 278–288, July 1973.

[27] P. Nicolas and G. Deloche, "Convolution computer processing of the brain electrical image transmission," *International Journal of Bio-Medical Computing*, vol. 7, no. 2, pp. 143 – 159, 1976.

[28] W. J. Freeman, "Use of spatial deconvolution to compensate for distortion of EEG by volume conduction," *IEEE Transactions on Biomedical Engineering*, vol. BME-27, no. 8, pp. 421–429, Aug 1980.

[29] P. L. Nunez, R. B. Silberstein *et al.*, "Comparison of high resolution EEG methods having different theoretical bases," *Brain Topography*, vol. 5, no. 4, pp. 361–364, Jun 1993.

[30] R. Srinivasan, P. L. Nunez *et al.*, "Spatial sampling and filtering of EEG with spline Laplacian to estimate cortical potential," *Brain Topography*, no. 8, pp. 355–366, 1996.

[31] M. Junghöfer, T. Elbert *et al.*, "Mapping EEG-potentials on the surface of the brain: A strategy for uncovering cortical sources," *Brain Topography*, vol. 9, no. 3, pp. 203–217, Mar 1997.

[32] C. Tenke and J. Kayser, "Reference-free quantification of EEG spectra: Combining current source density (CSD) and frequency principal components analysis (fPCA)," *Clinical Neurophysiology*, vol. 116, no. 12, pp. 2826 – 2846, 2005.

[33] D. Haor, R. Shavit *et al.*, "Back-projection cortical potential imaging: theory and results," *IEEE Transactions on medical imaging*, vol. 36, no. 7, 2017.

[34] Bin He, Yunhua Wang, and Dongsheng Wu, "Estimating cortical potentials from scalp EEGs in a realistically shaped inhomogeneous head model by means of the boundary element method," *IEEE Transactions on Biomedical Engineering*, vol. 46, no. 10, pp. 1264–1268, Oct 1999.

[35] Bin He, X. Zhang *et al.*, "Boundary element method-based cortical potential imaging of somatosensory evoked potentials using subjects' magnetic resonance images," *NeuroImage*, vol. 16, pp. 564–0576, Jul 2002.

[36] M. Clerc and J. Kybic, "Cortical mapping by Laplace–Cauchy transmission using a boundary element method," *Inverse Problems*, vol. 23, no. 6, 2007.

[37] A. Gevins, P. Brickett *et al.*, "Beyond topographic mapping: toward functional-anatomical imaging with 124-channel EEGs and 3-D MRIs," *Brain topography*, vol. 3, no. 1, pp. 53–64, 1990.

[38] A. S. Gevins and J. Le, "EEG spatial enhancement method and system," U.S. Patent 5 331 970, Jul. 26, 1994.

[39] ——, "EEG deblurring method and system for improved spatial detail," U.S. Patent 5 568 816, Oct. 29, 1996.

[40] L. Bourgeois, "A mixed formulation of quasi-reversibility to solve the Cauchy problem for Laplace's equation," *Inverse Problems*, vol. 21, no. 3, 2005.

[41] ——, "Convergence rates for the quasi-reversibility method to solve the Cauchy problem for Laplace's equation," *Inverse Problems*, vol. 22, no. 2, 2006.

[42] N. Koshev, N. Yavich *et al.*, "FEM-based scalp-to-cortex EEG data mapping via the solution of the Cauchy problem," *J. Inverse Ill-Posed Probl.*, vol. in print, 2020.

[43] G. Folland, *Introduction to partial differential equations*. Princeton Academic Press, 2001.

[44] G. Alessandrini, L. Rondi *et al.*, "The stability for the Cauchy problem for elliptic equations," *Inverse Problems*, vol. 25, no. 12, p. 123004, nov 2009.

[45] F. Brezzi and M. Fortin, *Mixed and Hybrid Finite Element Methods*. Berlin, Heidelberg: Springer-Verlag, 1991.

[46] O. C. Zienkiewicz and J. Z. Zhu, "The superconvergent patch recovery and a posteriori error estimates. part 2: Error estimates and adaptivity," *International Journal for Numerical Methods in Engineering*, vol. 33, no. 7, pp. 1365–1382, 1992.

[47] "MFEM: Modular finite element methods library," mfem.org.

[48] T. A. Davis, "A column pre-ordering strategy for the unsymmetric-pattern multifrontal method," *ACM Trans. Math. Softw.*, vol. 30, no. 2, p. 165–195, Jun. 2004.

[49] J. A. Reeger and B. Fornberg, "Numerical quadrature over the surface of a sphere," *Studies in Applied Mathematics*, vol. 137, no. 2, pp. 174–188, 2016.

[50] H. Si, "TetGen, a Delaunay-based quality tetrahedral mesh generator," *ACM Trans. on Mathematical Software*, vol. 41, no. 2, p. Article No.11, 2015.

[51] Q. Fang and D. Boas, "Tetrahedral mesh generation from volumetric binary and gray-scale images," in *Proceedings of International Symposium on Biomedical Imaging 2009*. IEEE, 2009, pp. 1142–1145.

[52] "FreeSurfer: an open source software suite for processing and analyzing (human) brain MRI images," http://surfer.nmr.mgh.harvard.edu/.

[53] R. Oostenveld, P. Fries *et al.*, "FieldTrip: Open source software for advanced analysis of MEG, EEG, and invasive electrophysiological data," *Computational Intelligence and Neuroscience*, vol. vol. 2011, Article ID 156869, 2011.

[54] G. Wahba, "Spline interpolation and smoothing on the sphere," *SIAM Journal on Scientific and Statistical Computing*, vol. 2, no. 1, pp. 5–16, 1981.

[55] F. Perrin, J. Pernier *et al.*, "Spherical splines for scalp potential and current density mapping," *Electroencephalography and clinical Neurophysiology*, no. 72, pp. 184–187, 1989.

[56] J. Kayser and C. Tenke, "Principal components analysis of Laplacian waveforms as a generic method for identifying ERP generator patterns: I. Evaluation with auditory oddball tasks," *Clinical Neurophysiology*, vol. 117, no. 2, pp. 348–368, 2005.

[57] "Kayser, J. (2009). Current source density (CSD) interpolation using spherical splines - CSD Toolbox (Version 1.1), New York State Psychiatric Institute: Division of Cognitive Neuroscience," http://psychophysiology.cpmc.columbia.edu/Software/CSDtoolbox.

[58] J. Dardé, A. Hannukainen, and N. Hyvönen, "An H_{div}-based mixed Quasi-Reversibility Method for solving elliptic Cauchy problems," *SIAM Journal on Numerical Analysis*, vol. 51, no. 4, pp. 2123–2148, 2013.

[59] I. Zacharov, R. Arslanov *et al.*, "Zhores—Petaflops supercomputer for data-driven modeling, machine learning and artificial intelligence installed in Skolkovo Institute of Science and Technology," *Open Eng.*, no. 9, pp. 512–520, 2019.